ORIGINAL PAPER

Molecular dynamics simulation of polypropylene: diffusion and sorption of H_2O, H_2O_2, H_2, O_2 and determination of the glass transition temperature

Fabian Deckers[1] · Karsten Rasim[2] · Christian Schröder[1,3]

Abstract

Molecular dynamics (MD) simulations in the canonical (NVT) and the isothermal-isobaric (NPT) ensemble using COMPASS III molecular force fields were performed to study the penetrant diffusion of water (H_2O), hydrogen peroxide (H_2O_2) and oxygen (O_2) in isotactic polypropylene (iPP) and hydrogen (H_2) in iPP and atactic polypropylene (aPP) for time intervals up to 11 ns and in the case of H_2O_2 up to 22 ns. We found robust cluster formation in the case of H_2O and H_2O_2. Further, the diffusion coefficients for all these systems were estimated by mean-square displacement analysis. Our results are consistent with previously published experimental and computational data except for the diffusion of H_2 in polypropylene where our results are one and two orders of magnitude higher, respectively. Grand Canonical Monte Carlo (GCMC) simulations were used to determine the sorption loading and saturation concentration of H_2O, O_2 and H_2 in iPP, where we find good agreement for H_2O with experimental results. By means of MD simulation the glass transition temperature (T_g) of iPP was estimated to 273.66 ± 4.21 K which is consistent with previously published experimental results.

Keywords Molecular dynamics simulation · Polypropylene · Diffusion · Sorption · Glass transition temperature

Introduction

The world's demand for the polymeric material polypropylene (PP) is the second largest, after polyethylene (PE), and it grows from year to year. In 2018 the global production volume amounted to 56 million tons and by 2026, it is forecasted that the production volume will reach 88 million tons [1]. In terms of sustainability, the goal must be to reduce this output significantly and to force the recycling and reuse of material. However, this requires the design of high quality and robust

✉ Christian Schröder
  christian.schroeder@fh-bielefeld.de;
  christian.schroeder@uni-bielefeld.de

  Fabian Deckers
  fabian.deckers@fh-bielefeld.de

1 Bielefeld Institute for Applied Materials Research, Bielefeld University of Applied Sciences, Interaktion 1, 33619 Bielefeld, Germany

2 Miele & Cie. KG, Carl-Miele-Straße 29, 33332 Gütersloh, Germany

3 Faculty of Physics, Bielefeld University, Universitätsstraße 4, 33615 Bielefeld, Germany

PP-based products that maintain their integrity over long times. Especially when used in moisture environments, e.g. for food packaging or as part of household appliances like washing machines, polymeric materials show aging and degradation behaviour that can significantly reduce their quality and lifetime. Responsible for this behaviour are catalytic reactions and autoxidation processes induced by oxygen (O_2) or reactive oxygen species (ROS) such as hydrogen peroxide (H_2O_2) producing molecules like water (H_2O) and hydrogen (H_2) as reaction products. When used in washing machines, H_2O as a molecule is even more important, since it serves as a carrier medium for laundry detergents and bleaching agents [2, 3]. In order to study such interactions on an atomistic level Molecular dynamics (MD) and Monte Carlo (MC) simulations have proven to be powerful computational tools. With increasing hardware specs and more advanced digital analysing methods, computational approaches play an important role in the process of guiding experimental developments and studying the complex interaction and behaviour of molecules in different polymer systems.

In 1989 and 1990 Trohalaki et al., Takeuchi and Okazaki, Takeuchi as well as Madkour et al. in 1992 performed pioneering studies of the penetrant diffusion of carbon dioxide

and O_2 in polyethylene (PE) by means of MD [4–8]. Until 1994 Boyd et al. and Müller-Plathe provided results on methane as a penetrant in PE [9–13], in polyisobutene (PIB) [9, 10, 12] and atactical polypropylene (aPP) [12, 14]. Furthermore, Müller-Plathe et al. studied the behaviour of O_2 and H_2 as diffusive penetrants in aPP and PIB [14–16] as well as helium in PIB [16].

The experimental determination of diffusive properties of H_2O and other polar penetrants in polyolefins is difficult due to the small solubility that is caused by the hydrophobic character of the polymeric host material. In contrast to this, MD and MC simulation methods provide excellent tools to study diffusive properties theoretically on an atomic scale. The first computational investigation of H_2O in PE was carried out by Tamai et al. in 1994 and 1995 [17, 18]. However, they modelled only a single H_2O molecule in a PE membrane. Tamai et al. further investigated the diffusion of five H_2O molecules in poly(dimethylsiloxane) (PDMS) and found an aggregation of these molecules due to the formation of hydrogen bonds between them. Moreover, it has been found that the diffusion coefficients of aggregated H_2O molecules compared to a single H_2O molecule in PDMS are smaller by a factor of 50 [17].

Further investigations of H_2O as a penetrant were carried out by Fukuda and Kuwajima in 1997 with one, three and ten H_2O molecules in PE. They found H_2O molecules aggregating and forming clusters of various sizes and the obtained diffusion coefficients were reduced by one order of magnitude compared to that of a single H_2O molecule [19]. Fukuda and Kuwajima extended their study of H_2O as a penetrant in aPP and isotactical polypropylene (iPP). Again, they found a clustering of the H_2O molecules in both systems. For iPP they found that the clustered structure is robust and maintained over several nanoseconds [20].

More recently in 2009 Chang-Gui et al. and in 2010 Rong et al. calculated the diffusion coefficient of O_2 in PP [21], PE, iPP and poly(vinyl chloride) (PVC) [22] by means of MD. Furthermore, by using a Grand canonical Monte Carlo (GCMC) approach they were able to determine the number of O_2 molecules absorbed in PP [21] and PE [22]. In 2013 Börjesson et al. calculated the solubility, diffusion coefficients, and the permeation of O_2 and H_2O in PE using an MD and MC approach [23]. In 2019 Sun et al. studied the diffusion behaviour of five different flavor organic molecules in low density polyethylene (LDPE) as well as the effects of the presence of these flavors on the diffusion of O_2 and H_2O by combined experimental and MD simulation studies. They found out that the presence of these flavors hinders the diffusion of O_2 and H_2O because of the smaller available free volume and negative interaction energies between O_2 and H_2O with the flavor molecules [24].

Due to its high chemical reactivity H_2O_2 plays an important role in many biological processes as well as in cleaning and pharmaceutical applications, e.g. as protection against microbes, as a bleaching agent and as a decontamination agent.

Technical applications in these areas typically use polymers since they are cheap, reliable, and light weighted as compared to other materials. However, exposed to H_2O_2 polymers suffer from degradation of the surface and the bulk [25–27]. Thus, understanding the interaction of H_2O_2 with a polymer matrix is important for the development of robust and inert polymer materials. The experimental analysis of such interaction is difficult since there are superimposing effects, e.g. one cannot disentangle desorption from diffusion effects. On the other hand, a computational analysis allows to disentangle such superimposing effects by studying the interactions of H_2O_2 within a polymer matrix solely.

There is little experimental results on the diffusivity of H_2O_2 in polymers available: In 1959, Dietrick and Meeks studied the permeability of H_2O_2 diluted in LDPE, PVC, polyester and polyvinylidene chloride [28]. In 2011, Radl et al. determined the diffusion coefficient and the saturation of H_2O_2 in PP, LDPE, PVC and glass. For PP they determined $D = 5.50 \cdot 10^{-9}$ cm^2/s for T = 298 K and $D = 2.00 \cdot 10^{-8}$ cm^2/s at T = 308 K, respectively. The results differ by a remarkably large factor of 3.6 [29]. In 2018, Tjell and Almdal studied the permeability of H_2O_2 in different commercially available water-swelled polyurethanes [25]. Recently, Yabuta et al. determined the diffusion coefficients in the range of $D \sim 10^{-8}$ cm^2/s for H_2O_2 in PE, chlorosulfonated PE, PVC, silicone and polyoxymethylene (POM) at 298 K in aeration experiments [26].

In this paper we provide molecular dynamics simulation results for small molecules in PP. Since commercially used PP is usually isotactic, the focus of our investigation is on iPP. We study the clustering behaviour of H_2O and for the first time of H_2O_2 using one and ten molecules within an iPP matrix for different time scales up to 11 ns and in the case of ten H_2O_2 molecules in iPP for up to 22 ns. The latter is necessary due to the observation of subdiffusive behaviour at short times. In addition, we calculate and compare the diffusion coefficients for H_2O, H_2O_2, O_2 and H_2 in iPP and for H_2 also in aPP. With respect to the glassy and rubbery state of PP and an expected strong temperature dependency of the diffusion coefficients, we calculated and compared the diffusion coefficient of O_2 for different temperatures. By means of GCMC sorption loadings and saturations of H_2O, O_2 and H_2 in iPP are estimated. Furthermore, we determined the glass transition temperature of iPP by means of MD simulations.

Simulation models and methodology

We used Materials Studio version 20.1 [30] for our simulation studies, including its pre-processing and post-processing capabilities. Constant temperature MD simulations have been carried out in the canonical ensemble (NVT) and in the isothermal-isobaric ensemble (NPT). Furthermore, we used the Grand canonical Monte Carlo (GCMC)

approach to determine the sorption loading of H_2O, O_2 and H_2 in isotactic polypropylene (iPP).

For the MD simulations the proper choice of the force field is crucial to obtain accurate results. The Condensed-phase Optimized Molecular Potentials for Atomistic Simulation Studies (COMPASS) force field [31] and the Polymer Consistent Forcefield (PCFF) [32, 33] are improvements of the Consistent Force Field (CFF) developed in the 1990's by Maple et al. [34–36]. These force fields are recommended for studies of soft materials like polymers or carbon-based systems [37–39]. In a direct comparison of COMPASS and PCFF, several authors report that COMPASS provides a better agreement with experimental results [40], is less erroneous, more reliable, delivers more uniform results [41], determines the steady-state density closer to the correct density and delivers smaller volatility in the calculation of mechanical properties [42].

The COMPASS force field was further improved to produce more reliable results and to be applicable to different materials systems [31, 43–46]. Thus, for our study we used the latest version COMPASS III [47].

Preparation of the polypropylene model system

For the construction of the iPP model systems and one aPP model system we used the Build Polymers tool of Materials Studio. After geometry optimization, a three-dimensional box with periodic boundary conditions is created via the Amorphous Cell module. The polymer chains are added into the box segment by segment while every new segment takes the interaction with previously placed atoms into account. Using this technique an amorphous polymer structure with a realistic conformation can be constructed, while minimizing the number of close contacts [40, 48]. In a final step we performed another geometry optimization of the simulation cell to avoid numerical instabilities.

We employ a nomenclature for our model systems similar to Fukuda and Kuwajima [19, 20]. A three-dimensional cell consisting of four isotactic polypropylene chains and each chain containing 50 monomers is referred to as iPP50(4). If the model contains additional small molecules, e.g. five O_2-molecules it is referred to as iPP50(4-5o). Table 1 shows the abbreviations used in the nomenclature

Table 1 List of abbreviations used in the nomenclature for the studied simulation cells

a	atactic
i	isotactic
w	water: H_2O
hp	hydrogen peroxide: H_2O_2
o	oxygen: O_2
h	hydrogen: H_2

for this study. Table 2 shows the different model systems that have been created and studied in this work.

Simulation details

All MD and GCMC simulations have been carried out using the Forcite Plus module of Materials Studio based on the COMPASS III force field. We obtained the best numerical stability using a time step length of 1 fs. To reduce the computational effort of the MD simulations, we used the group based electrostatic and van der Waals calculation approach as implemented in the Materials Studio software with a cut-off radius of 15.5 Å [30]. The temperature is controlled by a Nosé-Hoover thermostat with the default value for Q of 0.01. The maximum energy deviation between successive steps is set to the default value of 50,000 kcal/mol. In all GCMC simulations the electrostatic interactions were calculated using the Ewald summation method and a cut-off radius of 12.5 Å.

Equilibration

After construction the polypropylene chains do not uniformly occupy the space in the simulation cell and therefore the total energy of the system is far from equilibrium. To equilibrate the system, we performed MD simulations for 100 ps in the NVT ensemble at temperatures given in Table 2.

The iPP240(4) and iPP60(4) cells undergo an additional annealing procedure consisting of five heating and cooling cycles for further relaxation of internal stresses in the NPT ensemble at a pressure of 0 GPa. Each cycle consists of three heating and cooling stages over $\Delta T = 50$ K of which each stage has a duration of 100 fs.

Diffusion studies

In order to determine the diffusion coefficients of the different penetrants in the PP50 cells we have been performed 10 simulations per system in the NPT ensemble, each starting with random initial velocities and temperatures given in Table 2. The pressure was set to 10^{-4} GPa and the total simulation time was set to 11 ns except for iPP50(3-10hp) where it was set to 22 ns. Just like in the NVT ensemble, the temperature is controlled by a Nosé-Hoover thermostat, the pressure is controlled by a Berendsen barostat with a decay constant of 0.1 ps.

The diffusion coefficients D of the different penetrants in the polypropylene matrix are determined by the mean-square displacement (MSD) of the centre of mass:

$$MSD(t) = \langle |r_i(t) - r_i(0)|^2 \rangle, \tag{1}$$

where $r_i(0)$ is the i-th initial position and $r_i(t)$ is the position of the same molecule after a time t and $\langle \ldots \rangle$ denotes

Table 2 Systems and studies performed in this work

System	Temperature	Study
iPP50(3-1w)	298 K	Diffusive behaviour of H_2O in iPP
iPP50(3-10w)		
iPP50(3-1hp)		Diffusive behaviour of H_2O_2 in iPP
iPP50(3-10hp)		
iPP50(3-10o)	268, 298 and 328 K	Temperature dependant diffusive behaviour of O_2 in iPP
aPP50(3-10h)	298 K	Tacticity dependent diffusive behaviour of H_2 in aPP and iPP
iPP50(3-10h)		
iPP60(4)	263 – 303 K with $\Delta T = 5$ K	Sorption of different elements in iPP
iPP240(4)	243 – 303 K with $\Delta T = 5$ K	Determination of the glass transition temperature T_g of iPP

the ensemble average. For long enough times the Einstein relation [49] predicts a linear slope of the MSD vs. time for regular Brownian diffusion. Therefore, D can be determined by taking the slope of a linear fit to MSD(t) vs. t according to

$$D = \frac{1}{6} \sum_{i=1}^{N} \frac{\Delta MSD(\Delta t)}{\Delta t} \tag{2}$$

However, for short times one can observe local mobility followed by an anomalous diffusion behaviour where MSD(t) is proportional to t^n with $n < 1$ [50]. In order to simulate sufficiently long times this behaviour must be taken into account.

Sorption studies

After equilibration of the iPP60(4) cells by the above-described procedure, the Sorption Module of Materials Studio is used to carry out GCMC simulations. Within our simulation protocol the first 50,000 equilibration steps are used to adjust the fugacities and the temperature in the PP matrix followed by 150,000 production steps. The fugacities and the temperature in the PP matrix are kept constant as if the system was in open contact with an infinite sorbate reservoir at a fixed pressure of 101.325 kPa. During a production step a sorbate exchange with the reservoir as well as translation, rotation or torsion change of existing sorbate molecules are allowed to happen. The tool specific sample spacing is set to 25 steps and the grid spacing to 0.25 Å. For each system five simulations have been performed. With M_{pp} and M_s being the molecular weights of a polypropylene chain and one small-molecule sorbate, respectively, one can calculate the saturation content s in wt.% of the averaged penetrant loading l over all simulation steps. The factor n denotes the number of polypropylene chains within the simulation cell, i.e. for iPP60(4) n = 4.

$$s \, (wt.\%) = \frac{l \cdot M_s}{n \cdot M_{pp}} \cdot 100\% \tag{3}$$

Determination of the glass transition temperature

A common approach to determine one of the most important properties of amorphous polymers, the glass transition temperature, is to analyse the change in density or specific volume as a function of temperature [51]. While the volume increases linearly with increasing temperature due to the increasing molecular vibration, in amorphous or semi-crystalline materials one can find a change in that linear slope at the so-called glass transition temperature T_g distinguishing the glassy state (below T_g) from the rubbery state (above T_g). In the rubbery state the polymer chains can wiggle around causing the whole system to be more elastic. Using ten iPP240(4) model systems equilibrated at T = 303 K we determined the glass transition temperature according to the following procedure: We decreased the temperature from T = 303 K to T = 243 K in steps of $\Delta T = 5$ K. At T = 303 K we used random initial velocities, while for every following temperature the configurations and velocities of the previous simulation were used as initial conditions. The first 150 ps of every simulation were discarded for equilibration purposes, followed by 50 ps for determining the relation of the specific volume and temperature.

Results and discussion

Clustering of H_2O and H_2O_2

Fukuda and Kuwajima discovered and described the clustering of H_2O molecules in PP [20]. Here, we show that their results are reproducible within out setup. Furthermore, we performed simulations with H_2O_2 and obtain very similar results. Figure 1 shows snapshots of an iPP50(3-10w) cell in its initial configuration, after a 100 ps relaxation in the NVT ensemble and after 11 ns production-run in the NPT ensemble. Figure 2 shows snapshots at the same times for iPP50(3-10hp). After the production-run the formation of a compact cluster can be observed in the case of H_2O and H_2O_2, respectively. Interestingly, already after relaxation sub clusters of different sizes appear. For iPP50(3-10w) we
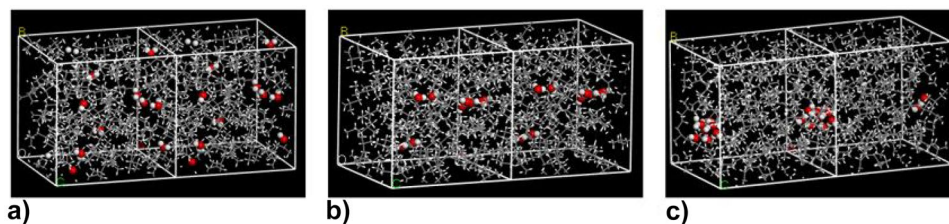
Fig. 1 Typical snapshots of the iPP50(3-10w) study, **a** in its initial configuration: The H_2O molecules are randomly distributed within the simulation box, **b** after a 100 ps NVT relaxation: The H_2O molecules form sub clusters containing five, three and two molecules, **c** after an 11 ns NPT production-run: A single compact cluster containing all ten H_2O molecules is formed

find three sub clusters containing five, three and two H_2O molecules and for iPP50(3-10hp) we find sub clusters of four, four and two H_2O_2 molecules, respectively. While each of the 11 ns production-runs results in compact clusters, the intermediate configurations after relaxation differ in the amount and size of the sub clusters formed. To prevent these random pre-clustering during the relaxation we set up a series of iPP50(3-10w) simulation cells in which the H_2O molecules were fixed in their position during relaxation. We refer to this model system as iPP50(3-10w)_fixed. During the NPT production-runs this constraint is lifted. Figure 3 shows snapshots of an NPT simulation of iPP50(3-10w)_fixed in its initial configuration, after 100 ps, after 1 ns and in its final configuration. After 1 ns there is a single

fully clustered configuration that persists until the end of the simulation at 11 ns. The same fast clustering after 1 ns we found for our other production-runs as well. However, we have to emphasize that this is not a general result but occurs due to the high H_2O concentration in our model system. For a larger simulation cell with a smaller concentration of H_2O we expect a longer formation time due to larger initial distances of the H_2O molecules. However, our results show that once the cluster is formed, it moves through the free volume in the iPP as an entity. For our analysis of diffusion coefficients, we have to distinguish between the motion of a single molecule not being influenced by the cluster forming process and the motion of a cluster of molecules which we will do in the following section.
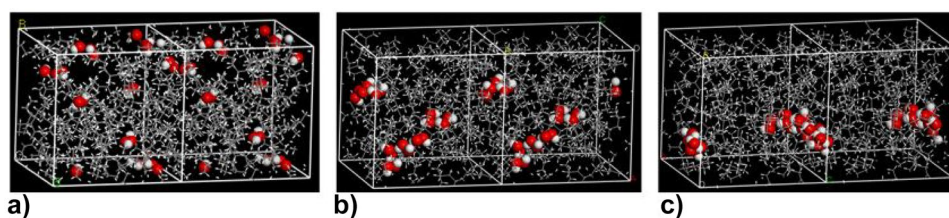

Fig. 2 Typical snapshots of the iPP50(3-10hp) study, **a** in its initial configuration: The H_2O_2 molecules are randomly distributed within the simulation box, **b** after a 100 ps NVT relaxing-run: The H_2O_2 molecules form sub clusters containing four, four and two molecules, **c** after an 11 ns NPT production-run: A single cluster containing all ten H_2O_2 molecules is formed
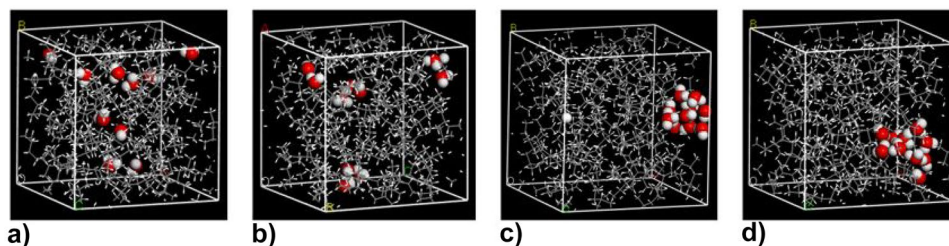

Fig. 3 Typical snapshots of the iPP50(3-10w)_fixed study: During the NVT relaxation the H_2O molecules are fixed in their positions while the iPP chains could relax, **a** the initial configuration for the 11 ns NPT production-run, **b** after 100 ps showing three sub clusters containing four, three and three H_2O molecules, **c** after 1 ns showing a single cluster containing all ten H_2O molecules, **d** final configuration after the 11 ns showing a single cluster
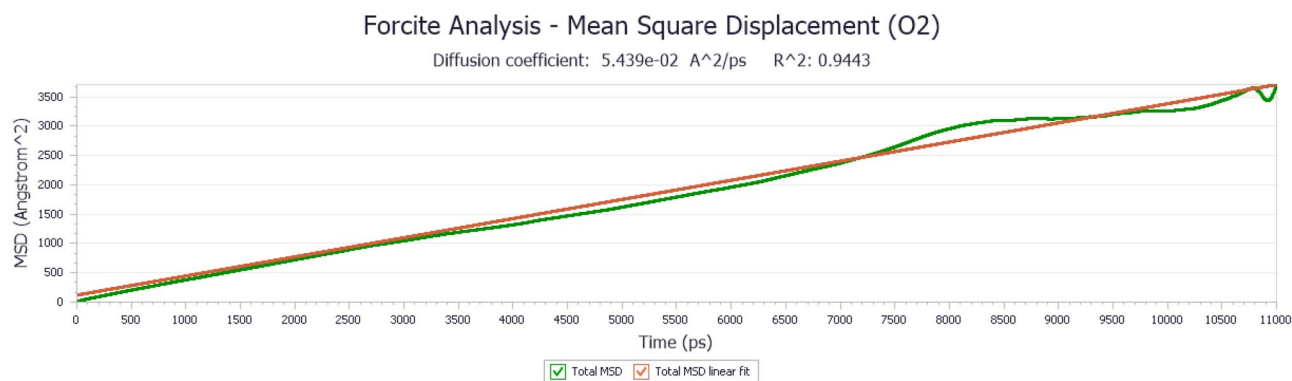
Forcite Analysis - Mean Square Displacement (O2)

Diffusion coefficient: 5.439e-02 A^2/ps   R^2: 0.9443

Fig. 4 MSD curve for the diffusion of O_2 in the system iPP50(3-10o) at 298 K

Determination of diffusion coefficients

We found 11 ns for the molecules H_2O, O_2 and H_2 and 22 ns for H_2O_2 to be sufficiently long enough times to apply the Einstein relation [49] to determine the diffusion coefficients by a linear fit of the MSD(t) curve (Eq. 2). As shown in Figs. 4, 5, 6 and 7 for non-polar penetrants such as O_2 and H_2 the linear fit works very well with $R^2 > 0.94$. In contrast to that, the fit to the MSD curves for the polar molecules H_2O and H_2O_2 (Figs. 4, 5, 6 and 7) yields R^2 values of less than 0.9 showing clear deviations from the linear behaviour, i.e. Brownian diffusion dynamics. This is caused by the interactions of the hydrophobic iPP with the polar penetrants as well as the interaction of the polar molecules among each other.

As described above, for our investigation of the polar molecules H_2O and H_2O_2 we want to distinguish between the diffusive behaviour of a single molecule and a cluster of molecules. Fukuda and Kuwajima [20] compared the systems aPP500(3-1w) with aPP500(3-3w) at 298 K where their calculated diffusion coefficient for the H_2O cluster of three molecules was one order of magnitude smaller than that for a single H_2O molecule. They also compared iPP500(3-10w)

with aPP500(3-10w). For one H_2O molecule in aPP their diffusion coefficients lie in the order of 10^{-6} cm^2/s which is in good agreement with our results for iPP. Their results for ten H_2O molecules forming a cluster and moving in iPP are of the order of 10^{-7} cm^2/s which is also in agreement with our results (see Table 3).

Just as Fukuda and Kuwajima [20], we determined diffusion coefficients for the time intervals 0–6, 6–11 and 0–11 ns. Furthermore, we used the time interval of 0–1 ns in order to investigate the influence of the cluster formation process, and in addition, we have determined the D values for one H_2O molecule in iPP as well. Note that determining D for a specified time interval does not include any data of other time intervals, i.e. determining D in the time interval 6–11 ns is based on the evaluation of a 5 ns long run with initial coordinates and velocities at t = 6 ns. In Table 3 we show a comparison of the different simulations for H_2O in iPP and the derived diffusion coefficients. The D values are averaged over ten MD runs. Figures 8, 9, and 10 shows the associated averaged D values of the ten runs together with their standard deviations.

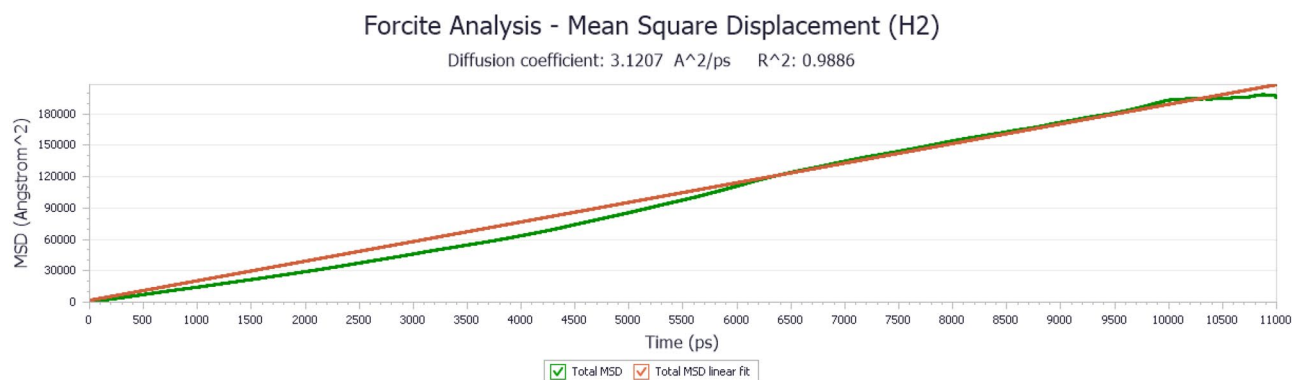The averaged diffusion coefficient for a single H_2O molecule (iPP50(3-1w)) ranges from $2.9 \cdot 10^{-6}$ to $5.8 \cdot$

Forcite Analysis - Mean Square Displacement (H2)

Diffusion coefficient: 3.1207 A^2/ps   R^2: 0.9886

Fig. 5 MSD curve for the diffusion of H_2 in the system iPP50(3-10h) at 298 K

Forcite Analysis - Mean Square Displacement (H2O)

Diffusion coefficient: 1.532e-03 A^2/ps   R^2: 0.8692
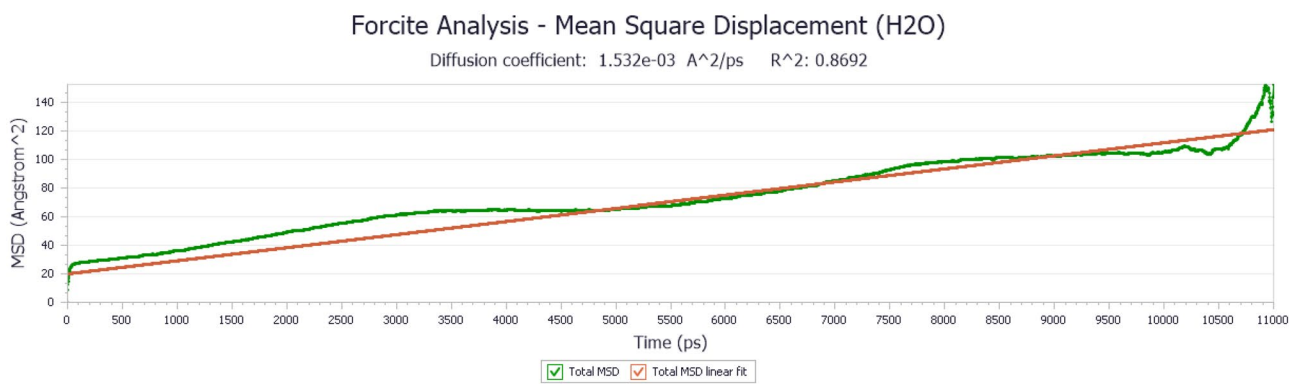
Fig. 6 MSD curve for the diffusion of H_2O in the system iPP50(3-10w) at 298 K

Forcite Analysis - Mean Square Displacement (H2O2)

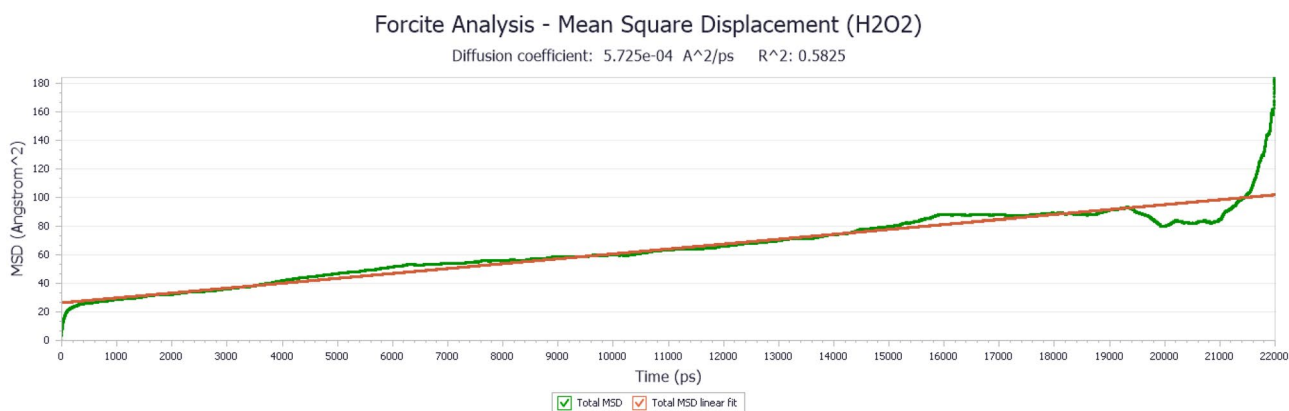Diffusion coefficient: 5.725e-04 A^2/ps   R^2: 0.5825

Fig. 7 MSD curve for the diffusion of H_2O_2 in the system iPP50(3-10hp) at 298 K

10^{-6} cm^2/s which is one order of magnitude higher than the average value for ten H_2O molecules (iPP50(3-10w)) which ranges from $1.0 \cdot 10^{-7}$ to $3.0 \cdot 10^{-7}$ cm^2/s. There are no significant differences between D of iPP50(3-10w) and

Table 3 Comparison of the calculated diffusion coefficients for different time intervals for H_2O in iPP at 298 K

System	Time intervals of the run (ns)	D (10^{-6} cm^2/s)
iPP50(3-1w)	0–1	3.620
	0–6	2.919
	6–11	3.071
	0–11	5.753
iPP50(3-10w)	0–1	0.142
	0–6	0.103
	6–11	0.284
	0–11	0.298
iPP50(3-10w)_fixed	0–1	0.258
	0–6	0.239
	6–11	0.307
	0–11	0.389

iPP50(3-10w)_fixed, where for the latter we find values ranging from $2.4 \cdot 10^{-7}$ to $3.9 \cdot 10^{-7}$ cm^2/s. Because of the very fast cluster formation process, even for the first ns in iPP50(3-10w)_fixed there is no measurable influence on D compared to 6 or 11 ns.

A possible solution to to distinguish between the diffusion of single H_2O molecules during the cluster formation and the diffusion of an H_2O cluster as an entity in a single simulation, is a study of much larger simulation cells with a smaller concentration of H_2O so that the cluster formation takes longer and thus the diffusion coefficients can be calculated during the cluster forming process more precisely.

For iPP50(3-1w) and for iPP50(3-10w)_fixed there are no significant differences of the standard deviations for the D values across different simulations observable. However, for iPP50(3-10w) the standard deviation is smaller at smaller times, i.e. 1 ns and 6 ns compared to larger times, i.e. 6–11 ns and 11 ns. For iPP50(3-10w)_fixed we expected more volatility at shorter times since the H_2O molecules are excluded from the equilibration process. When comparing the two equilibrated systems containing one and ten H_2O molecules, we find a smaller standard deviation at shorter times

Fig. 8 Average diffusion coefficients with standard deviations from ten NPT-MD simulations of iPP50(3-1w) calculated from the MSD for different time intervals at 298 K
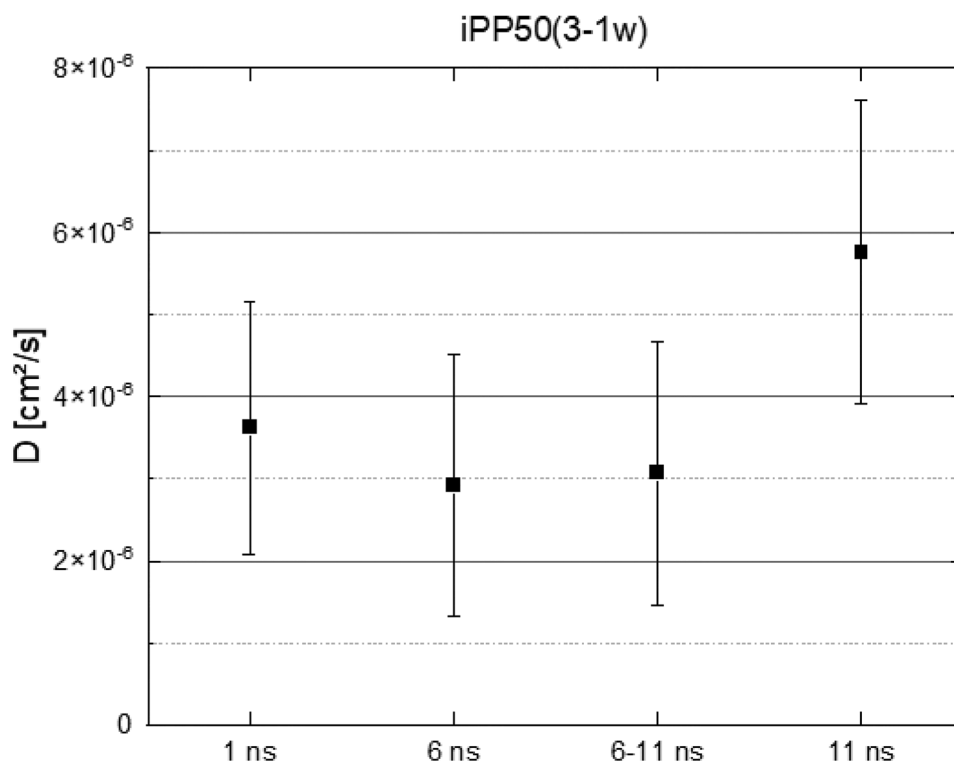

in iPP50(3-10w) which is due to the better statistics when averaging over ten (independent) H_2O molecules instead of one. For larger times this effect vanishes because of the correlated motion of the clustered H_2O molecules as an entity.

For H_2O_2 we find diffusion coefficients in the range of 10^{-6} for a single and 10^{-8} cm²/s for ten H_2O_2 molecules. The results for the two systems are shown in Table 4 and Figs. 11 and 12. For a single H_2O_2 molecule the diffusion

Fig. 9 Average diffusion coefficients with standard deviations from ten NPT-MD simulations of iPP50(3-10w) calculated from the MSD for different time intervals at 298 K
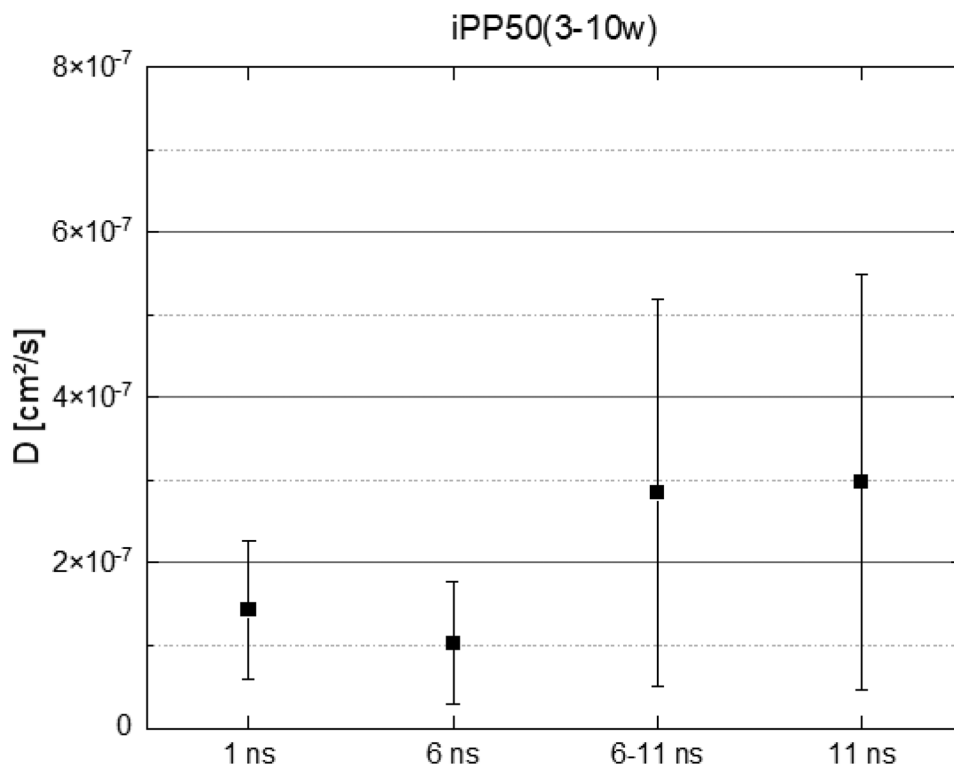
Fig. 10 Average diffusion coefficients with standard deviations from ten NPT-MD simulations of iPP50(3-10w)_fixed calculated from the MSD for different time intervals at 298 K
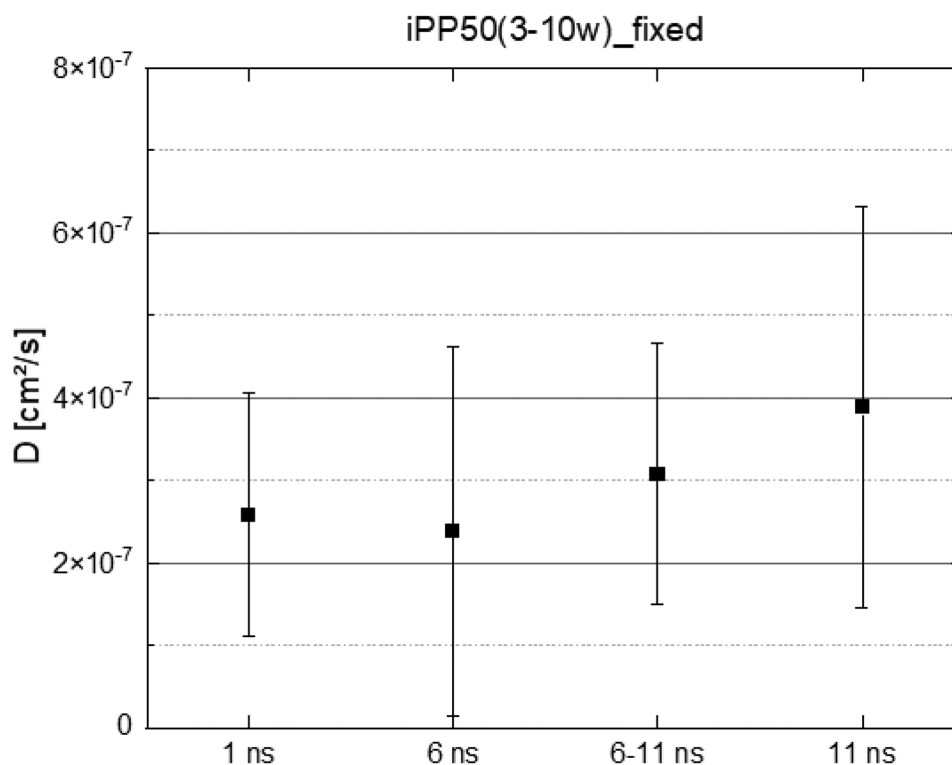
coefficient ranges from 3.4 to $6.8 \cdot 10^{-6}$ cm^2/s. The standard deviation of the longer time intervals 6–11 and 0–11 ns are very large compared to the results of ten H_2O_2 molecules and even compared to the result of a single H_2O molecule. This is consistent with the expected stronger interactions of the hydrophobic PP chains with the more polar penetrant H_2O_2 as compared to H_2O [52, 53]. For ten H_2O_2 molecules D ranges between 2.3 and $8.6 \cdot 10^{-8}$ cm^2/s and the standard deviations are much smaller due to the better statistics just like in the case of ten H_2O molecules. The only experimental value we can compare our result with was published by Radl et al. [29]. They determined the diffusion coefficient of H_2O_2 in PP at 298 K and found $D = 5.50 \cdot 10^{-9}$ cm^2/s which is one order of magnitude smaller than our value. We attribute this discrepancy to the difference of our simulation procedure to the experimental procedure they used. Radl et al. used fully saturated strips of PP in an aqueous 30% (w/w) H_2O_2 solution and determined the diffusion coefficient by measuring the desorption of H_2O_2 over time. In contrast to this our MD simulations are idealized in the sense that we only consider motion of H_2O_2 within the surrounding polymer matrix. Further, we calculated the motion of the H_2O_2 molecules within the polymer matrix only for several ns while the diffusion coefficient in the experimental approach was measured by desorption for which the H_2O_2 molecules must overcome the surface energy barrier before they get measured. This process could lead to a significantly lower diffusion rate as compared to the diffusion rate in the

bulk material. Nevertheless, our computationally determined diffusion coefficients for H_2O_2 in PP are useful as a reference for future theoretical and experimental studies.

Due to its reactive character O_2 generally plays an important role in damaging and aging processes of polymers. Apart from chemical reactions it is vital to know the temperature dependent transport properties of the molecule within a polymer matrix. In case of iPP we expect an increase of the transport properties at higher temperatures where the material is getting softer. Therefore, we did a temperature-dependant study at 268 K where iPP is more rigid, at room

Table 4 Comparison of the calculated diffusion coefficients for different time intervals for H_2O_2 in iPP at 298 K

System	Time intervals of the run (ns)	D (10^{-6} cm^2/s)
iPP50(3-1hp)	0–1	3.356
	0–6	3.534
	6–11	6.371
	0–11	6.812
iPP50(3-10hp)	0–1	0.072
	0–6	0.029
	6–11	0.086
	0–11	0.023
	11–22	0.027
	0–22	0.050

Fig. 11 Average diffusion coefficients with standard deviations from ten NPT-MD simulations of iPP50(3-1hp)_fixed calculated from the MSD for different time intervals at 298 K
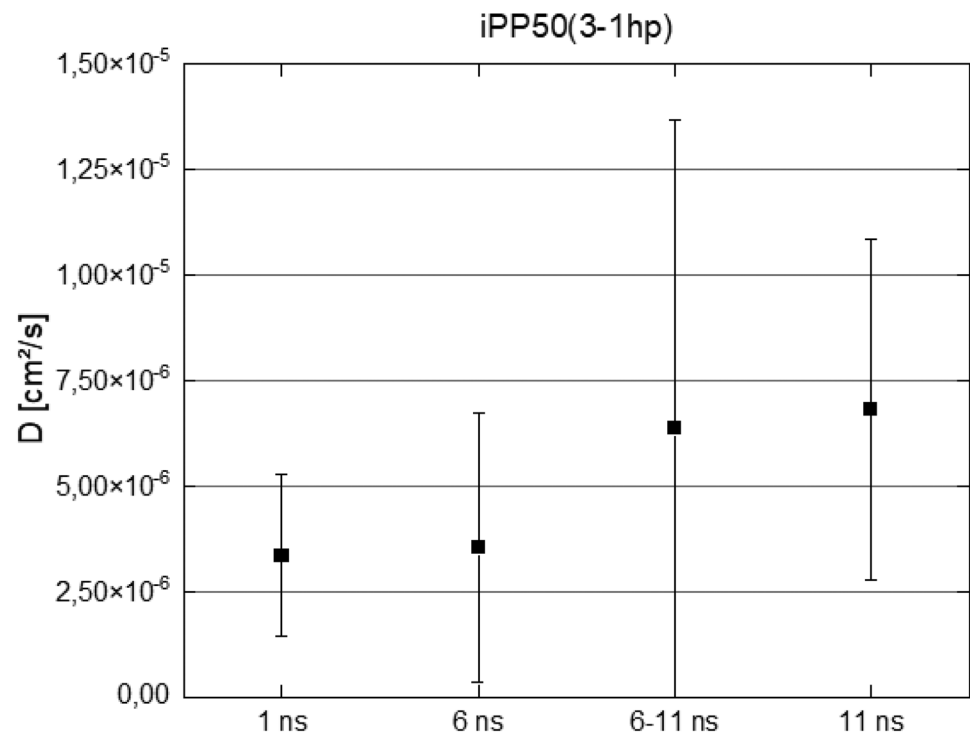

temperature, i.e. 298 K, and at 328 K where iPP is softer. We picked room temperature as a reference temperature because at this temperature we can compare our results to previously published simulational and experimental results. In Table 5 we show our results for the diffusion coefficients

for the different simulation runs for the non-polar penetrant O_2 in iPP. Figures 13, 14, and 15 shows the statistical evaluation of the determined D values. For iPP50(3-10o) at 298 K our averaged D values range from $5.7 \cdot 10^{-6}$ to $8.2 \cdot 10^{-6}$ cm^2/s and show a significantly smaller standard deviation

Fig. 12 Average diffusion coefficients with standard deviations from ten NPT-MD simulations of iPP50(3-10hp)_fixed calculated from the MSD for different time intervals at 298 K
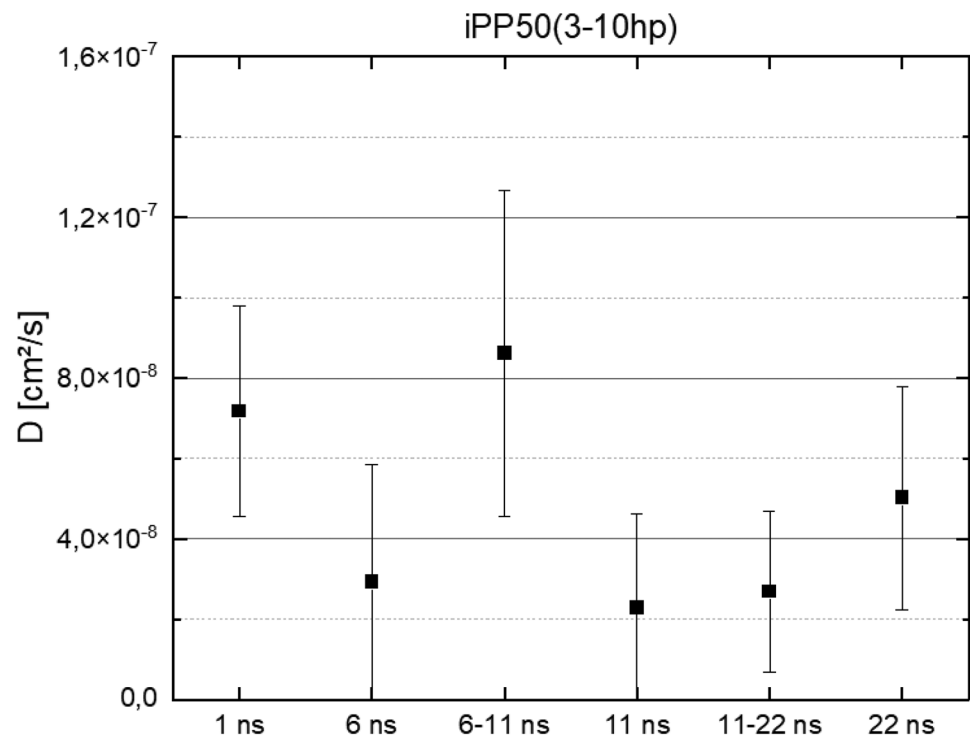
Table 5 Diffusion coefficient results of iPP50(3-10o) at 268 K, 298 K, and 328 K

System	Time intervals of the run (ns)	D (10^{-6} cm^2/s)
iPP50(3-10o) at 268 K	0–1	2.12
	0–6	2.37
	6–11	1.98
	0–11	2.29
iPP50(3-10o) at 298 K	0–1	6.08
	0–6	5.66
	6–11	5.93
	0–11	8.17
iPP50(3-10o) at 328 K	0–1	13.88
	0–6	16.16
	6–11	15.15
	0–11	17.04

compared to H_2O and H_2O_2. This is in good agreement with previously analysed O_2 diffusion in polypropylene by MD and experimentally. For atactical PP Müller-Plathe calculated D values for O_2 via MD simulations. Referring to our nomenclature he studied the system aPP76(1-8o) at T = 300 K and finds D = 4.04 · 10^{-6} cm^2/s [14]. Rong et al. determined a value of D = 3.688 · 10^{-6} cm^2/s for iPP60(4-2o) at T = 298 K [22]. Experimental values for D of the order of 10^{-7} cm^2/s at T = 298 K have been obtained by Kiryushkin and Gromov, and Eken et al. [54, 55].

We have determined the average O_2 diffusion coefficient for T = 268 K in the range of 2.0 · 10^{-6} to 2.4 · 10^{-6} cm^2/s. In comparison, for higher temperatures, i.e. 298 K and 328 K, one can clearly see that D is increased by a factor of three for T = 298 K and further increased by a factor of seven at T = 328 K. This is consistent with the expected higher mobility of the penetrants when iPP becomes softer and with the finding of Chang-Gui et al. that D increases for O_2 in PP with increasing temperature [21].

Comparing the widths of the standard deviations for the different temperatures shows the smallest at 268 K which indicates that the more rigid state also leads to more uniform results.

As pointed out in the beginning, H_2 appears as a reaction product of chemical reactions when H_2O_2 is involved. We therefore investigated its mobility in iPP at 298 K as well (see Table 6 and Figs. 16 and 17). For aPP76(1-8h) at 300 K Müller-Plathe determined a value of 4.35 · 10-5 cm²/s by means of MD simulations [14] using the class I force field GROMOS [56]. In comparison, we obtained our results by using the class II force field COMPASS and find a D value which is larger by factor of six in the range of 2.4 · 10^{-4} to 2.7 · 10^{-4} cm^2/s. In order to find out whether the tacticity of PP could cause such a difference we did another calculation using an aPP50(3-10 h) simulation cell. Here, we find D in the range of 2.0 · 10^{-4} to 2.4 · 10^{-4} cm^2/s which shows that the tacticity alone cannot explain the discrepancies. We therefore conclude that the deviation is caused by the choice

Fig. 13 Average diffusion coefficients with standard deviations from ten NPT-MD simulations of iPP50(3-10o) at 268 K calculated from the MSD for different time intervals
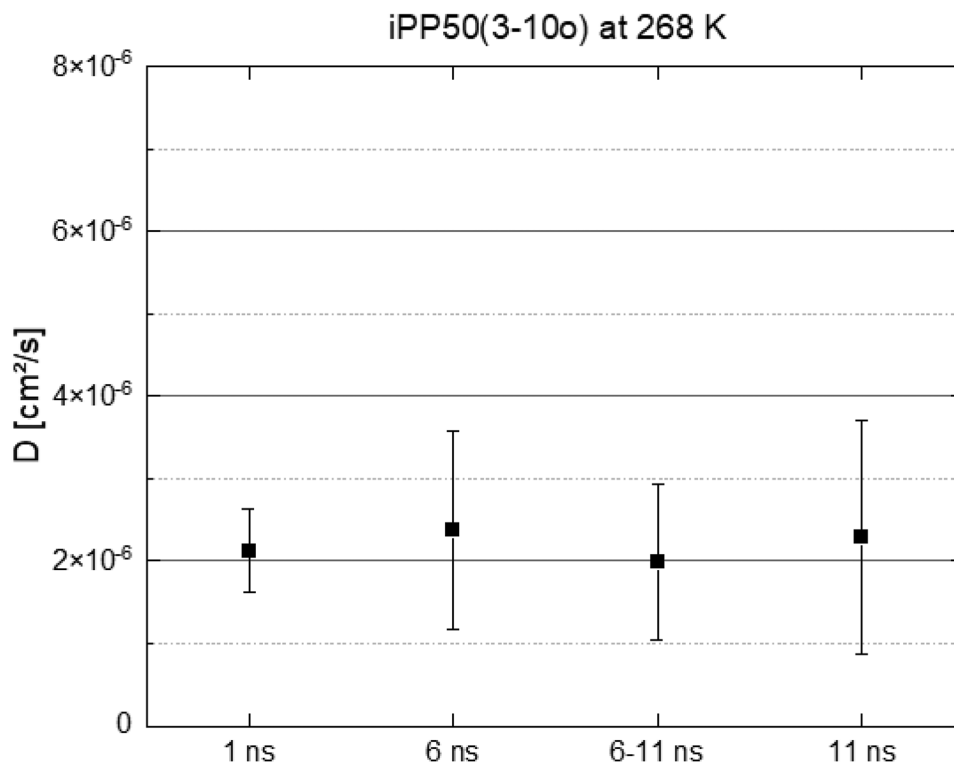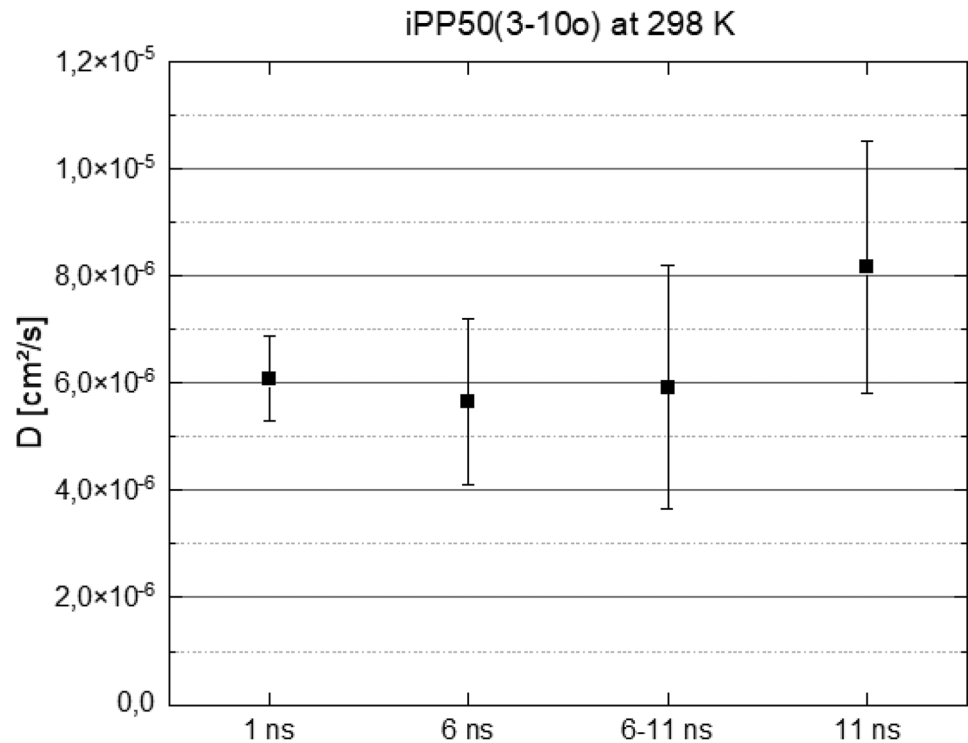
Fig. 14 Average diffusion coefficients with standard deviations from ten NPT-MD simulations of iPP50(3-10o) at 298 K calculated from the MSD for different time intervals

of the force fields. The only experimental result obtained by Jeschke and Stuart is $6.6 \cdot 10^{-6}$ cm^2/s for H$_2$ diffusion in aPP and $3.0 \cdot 10^{-6}$ cm^2/s in iPP, both at 293 K. Their experimental setup comprised two gas compartments separated by a thin PP foil. While one chamber is vacuumed, the other is filled with H$_2$-gas and the change in pressure was used to determine the diffusion coefficient [57]. In comparison our results are two orders of magnitude larger. We attribute this discrepancy to the idealized setup in our MD simulation. Like our previous results on H$_2$O$_2$, we only take

Fig. 15 Average diffusion coefficients with standard deviations from ten NPT-MD simulations of iPP50(3-10o) at 328 K calculated from the MSD for different time intervals
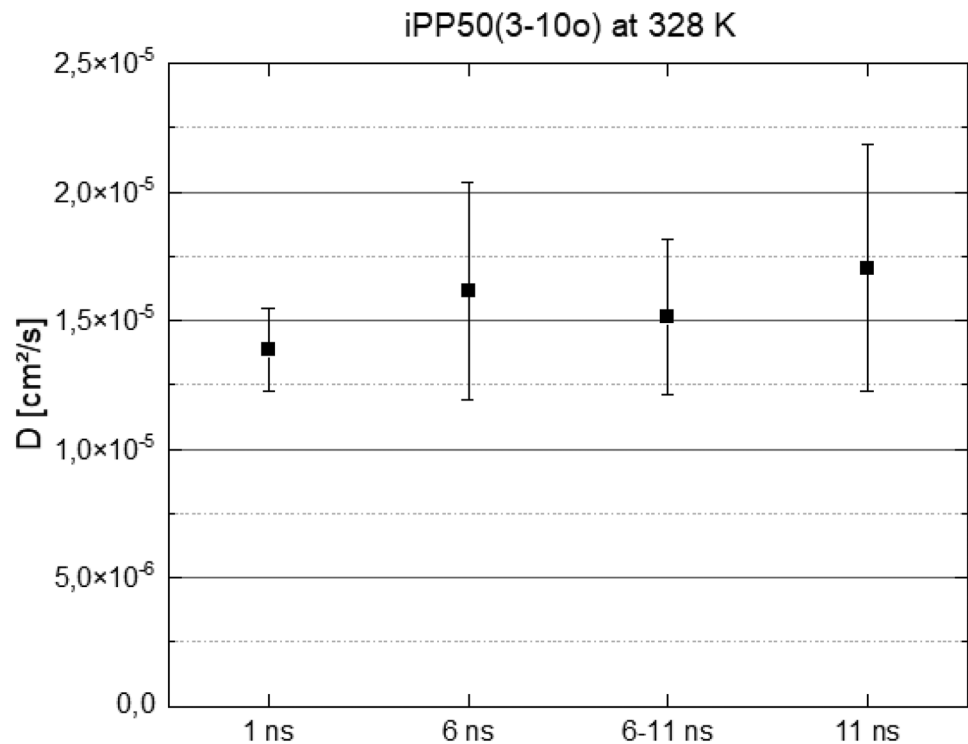
Table 6 Comparison of the calculated diffusion coefficients for different time intervals for H_2 in iPP at 298 K

System	Time intervals of the run (ns)	D (10^{-4} cm^2/s)
iPP50(3-10h)	0–1	2.39
	0–6	2.68
	6–11	2.38
	0–11	2.71
aPP50(3-10h)	0–1	2.44
	0–6	2.21
	6–11	2.31
	0–11	2.03

the interaction effects of H_2 within the polymer matrix into account while the experimental setup additionally took sorption and desorption of the H_2 molecules into account which decreases the measured diffusion coefficient.

Sorption loading analysis

An important property that characterizes the durability of the surface and bulk of polymeric materials is the absorption of and saturation with small molecules. We performed GCMC simulations comparing the free energy of a molecule in a gas reservoir with the state of it being in the polymer matrix. Figures 18, 19, and 20 shows the average loadings and their

standard deviations obtained by performing five GCMC simulations for H_2O, O_2 and H_2 in iPP60(4), respectively. We used 150,000 MC samples per temperature. Table 7 shows the average number of absorbed molecules and the resulting saturation calculated by Eq. 3.

As for PP being a highly hydrophobic material often used in the packaging industry to preserve food from getting in contact with moisture, the absorption of H_2O in PP is very small. Therefore, the exact determination of the saturation is challenging on the one hand but provides useful information for industrial applications on the other hand. The average loading of H_2O molecules in our iPP system ranges between 0.037 and 0.140 which corresponds to a saturation between 0.007 and 0.025 wt.% over all simulated temperatures from 263 to 303 K. There are only a few experimental results in the literature to compare with. Kahraman and Abu-Sharkh, Deng et al. and Mat-Shayuti et al. immersed polypropylene samples in distilled water for several months at room temperature [58], for one month at 296 K [59] as well as for 49 days at 296 K and for 7 days at 373 K [60]. Karahman and Abu-Sharkh reported that the moisture uptake was negligible and not significant enough to be published. For 296 K Deng et al. found a saturation of 0.03 wt.% and Mat-Shayuti et al. of 0.064 wt.%. At 373 K Mat-Shayuti et al. found a saturation of 0.571 wt.%. Our simulated results are consistent with the experimental results and show very limited H_2O uptake and no significant change with increasing or decreasing temperatures at and around room temperature.

Fig. 16 Average diffusion coefficients with standard deviations from ten NPT-MD simulations of iPP50(3-10h) calculated from the MSD for different time intervals at 298 K
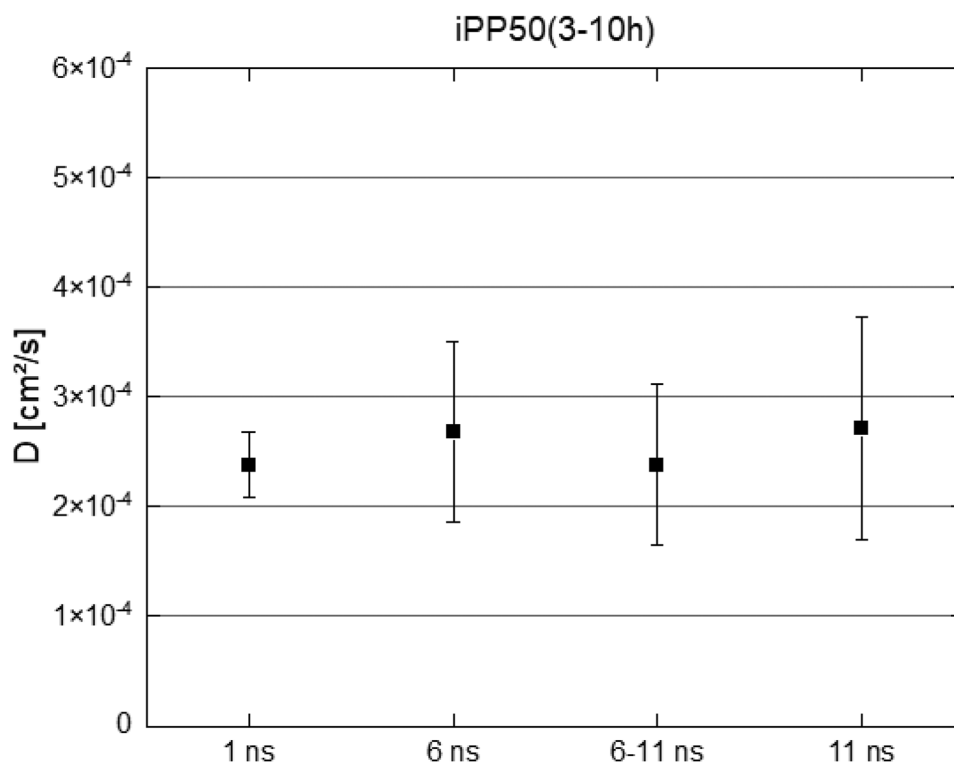
Fig. 17 Average diffusion coefficients with standard deviations from ten NPT-MD simulations of aPP50(3-10h) calculated from the MSD for different time intervals at 298 K
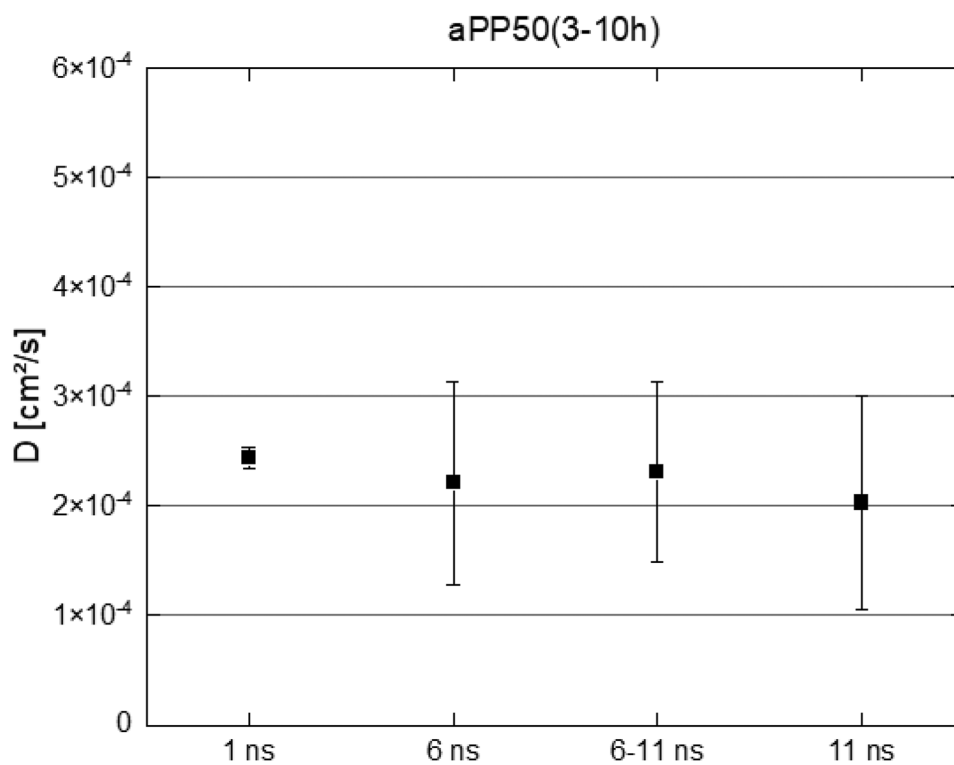

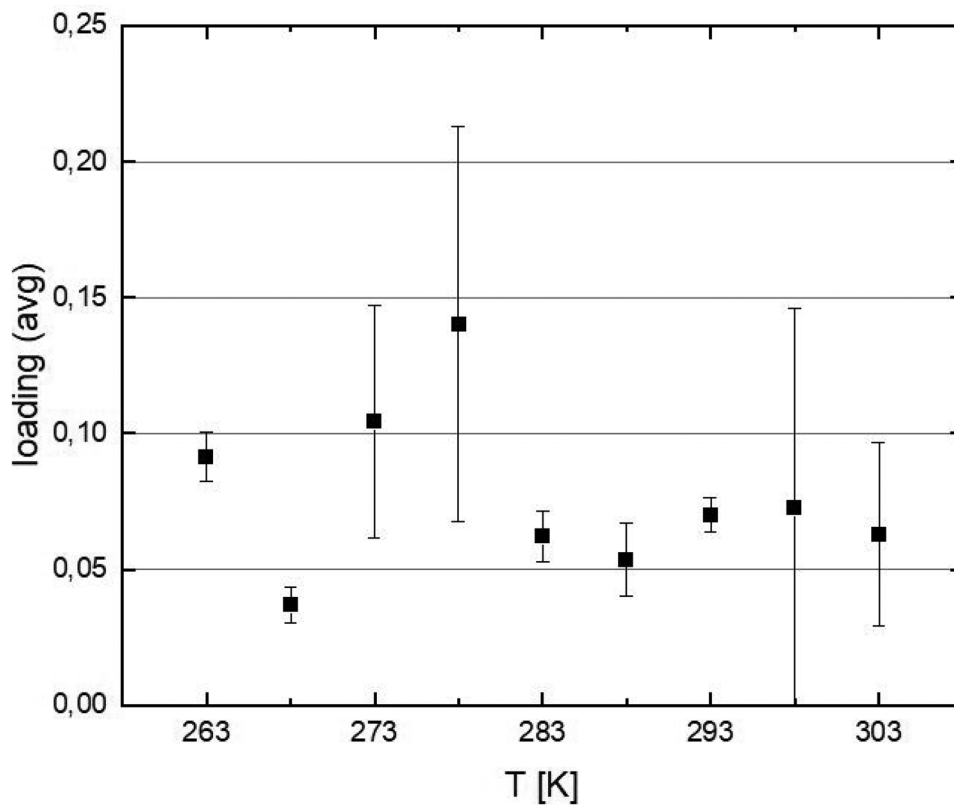**Fig. 18** The calculated loadings of H_2O molecules in iPP60(4) for five GCMC-runs

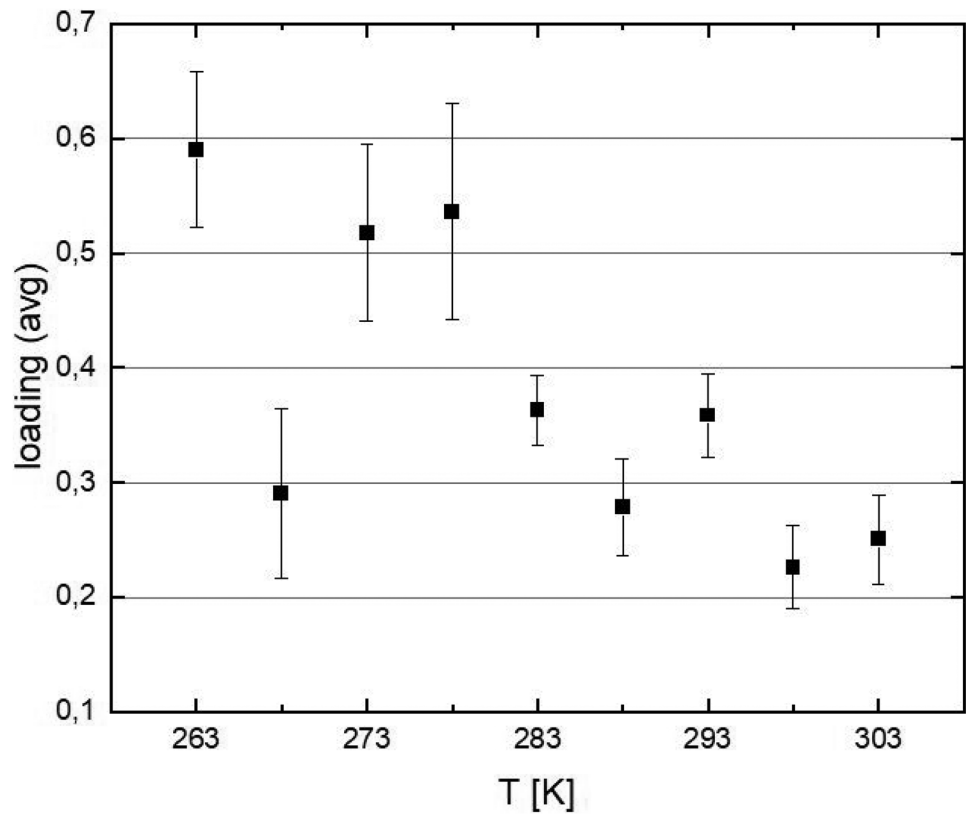**Fig. 19** The calculated loadings of O_2 molecules in iPP60(4) for five GCMC-runs

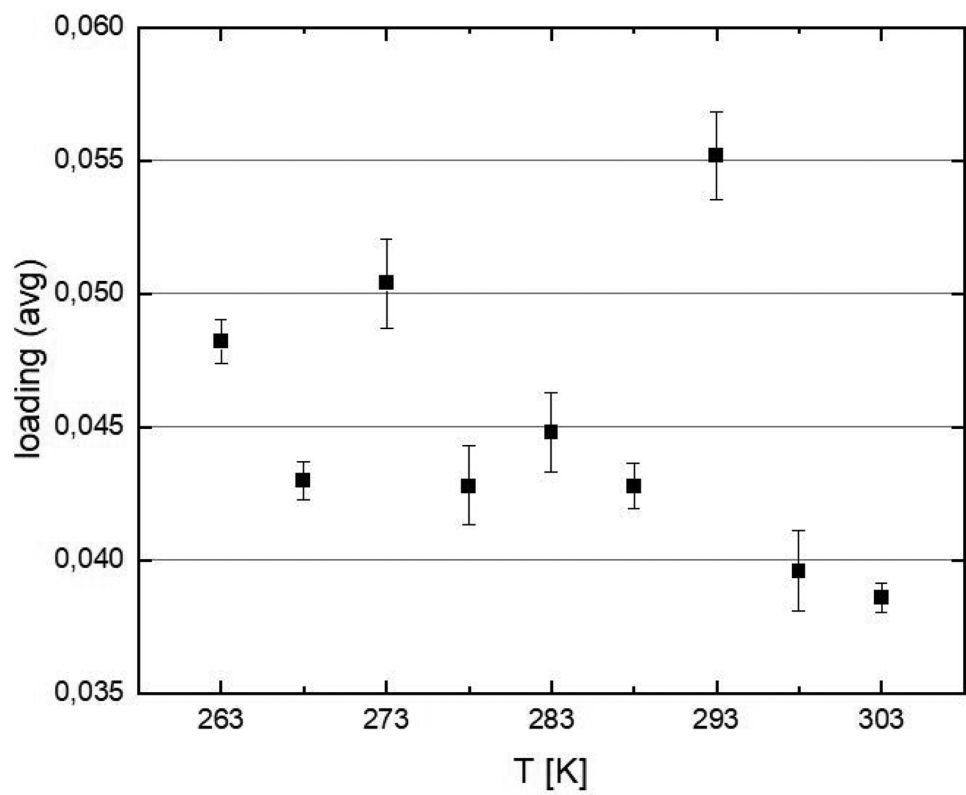**Fig. 20** The calculated loadings of H_2 molecules in iPP60(4) for five GCMC-runs

Table 7 Averaged number of absorbed H_2O, O_2 and H_2 molecules over five GCMC runs in iPP60(4) and resulting saturation values

Temperature (K)	263	268	273	278	283	288	293	298	303
loading of H_2O	0.091	0.037	0.104	0.140	0.062	0.054	0.070	0.072	0.063
Saturation of H_2O (wt.%)	0.01626	0.00655	0.01857	0.02494	0.01103	0.00954	0.0125	0.01288	0.01117
loading of O_2	0.590	0.290	0.518	0.536	0.363	0.278	0.358	0.227	0.250
Saturation of O_2 (wt.%)	0.18619	0.09164	0.16334	0.16921	0.11456	0.08786	0.11310	0.07151	0.07902
loading of H_2	0.048	0.043	0.050	0.043	0.045	0.043	0.055	0.040	0.039
Saturation of H_2 (wt.%)	0.00096	0.00086	0.00100	0.00085	0.00089	0.00085	0.00110	0.00079	0.00077

Experimental sorption studies of O_2 in polymers are generally difficult because of autoxidation processes taking place as soon as O_2 diffuses into a polymer like PP. Except for T = 268 K, the loading and saturation values obtained by GCMC simulations for O_2 in iPP show a decreasing trend with increasing temperature. This is consistent with the findings of Chang-Gui et al. and Rong et al. for O_2 sorption in PP [21] and PE [22]. The interaction and therefore the binding forces between the polymer and O_2 decreases with increasing temperature. We find an averaged saturation of O_2 of 0.186 wt.% at 263 K and 0.079 wt.% at 303 K, however with a large standard deviation.

In contrast to that, the loading values and the standard deviations for H_2 are smaller. This is expected because the interaction force between iPP and O_2 is much larger since more valence electrons are involved. Here, again a decreasing trend of loading and saturation with increasing temperature is visible, except for the value at 293 K where we find the highest saturation value of 0.00110 wt.%. The saturation of H_2 is 0.00096 wt.% at 263 K and 0.00077 wt.% at 303 K.

Determination of the glass transition temperature

For different types of polypropylene Cowie found experimentally an asymptotic increase of T_g with the molecular weight saturating at weights of 10^4 and above [61] which is equivalent to a degree of polymerisation of ≈ 238. By means of MD simulations Yu et al. found for chain lengths longer than ~200 units that the glass transition temperature is insensitive to further increasing the chain length [62]. Given this we performed simulations using a model system with a chain length of 240.

In Fig. 21 we show a plot of the density per cell of iPP240(4) for a 200 ps simulation at 303 K. In total, we performed 10 simulation runs with different initial configurations (see Ch. 2.1) and the average density and the specific volume V_{spec} were calculated using the last 50 ps of each run at each temperature. Figure 22 shows the averaged specific volumes including standard deviations vs. temperature with $R^2 = 0.997$. To obtain a value for T_g we fitted the data simultaneously to two piecewise linear functions using a
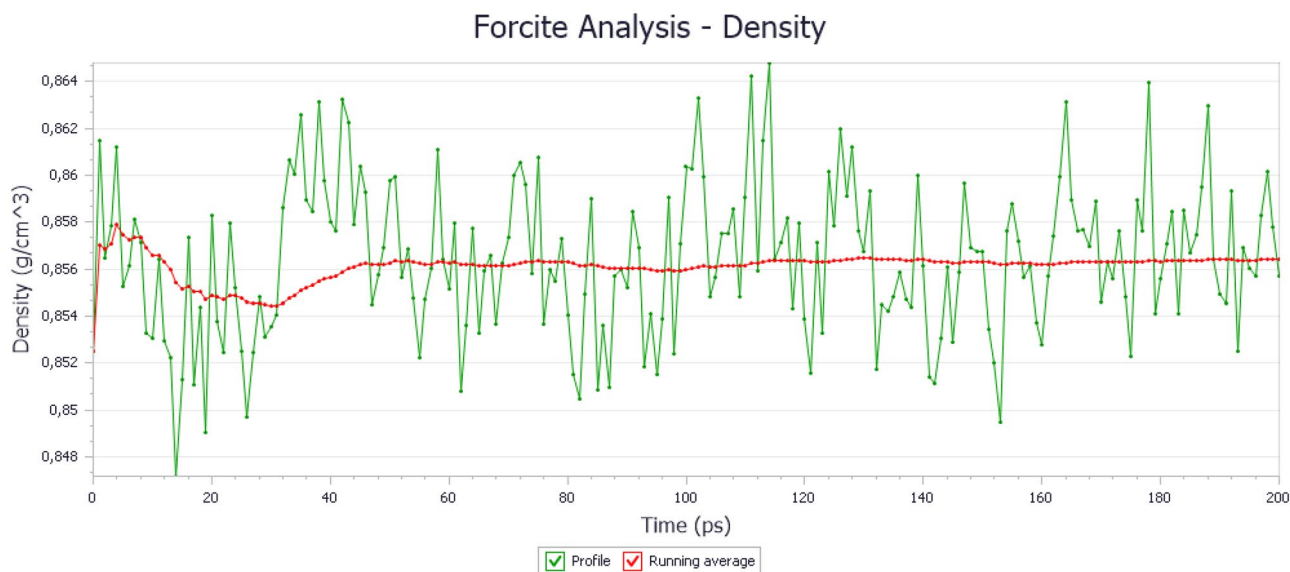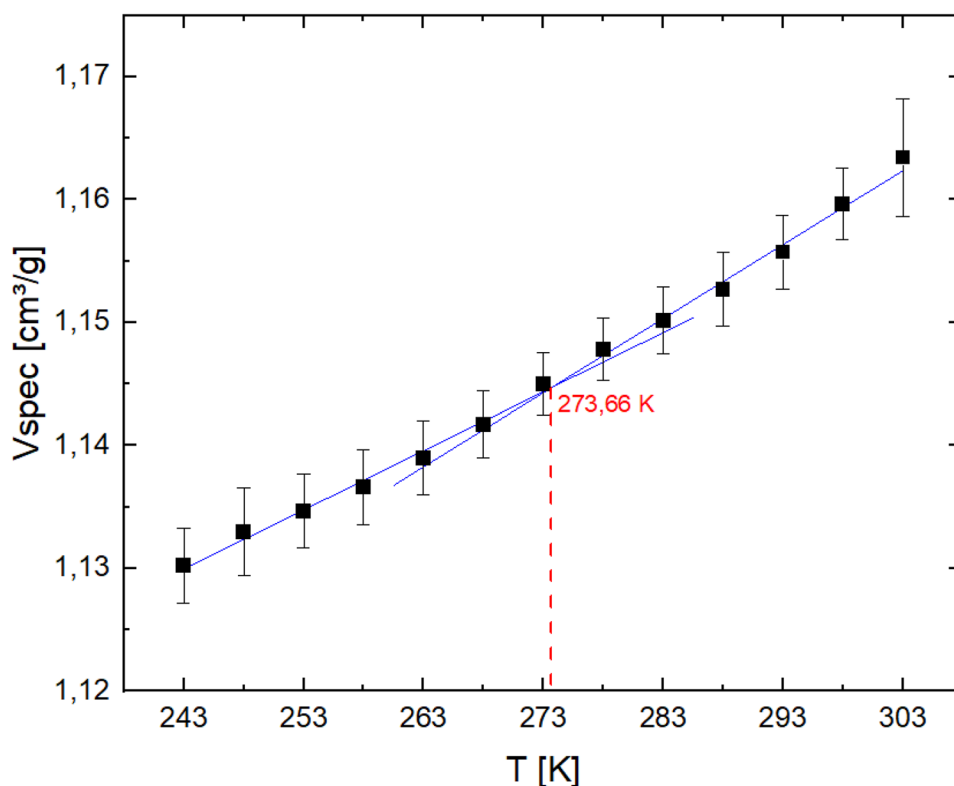

Fig. 21 Density of iPP240(4) over a 200 ps NPT simulation at 303 K

Fig. 22 Determination of T_g using a simultaneous least-square fit of two piecewise linear functions to the averaged specific volume of ten runs per temperature for iPP240(4)

least square fitting routine [63]. As a result, we find the intersection at $T_g = 273.66 \pm 4.21$ K which is in good agreement with the experimental findings shown in Table 8. Two of the published simulational results differ by over 100 K, namely $T_g = 248$ K [62] and $T_g = 364$ K [64], respectively. One can argue that the standard deviation for our results is quite large. However, none of the referenced experimental and simulational results provided any standard deviation at all.

Table 8 Literature data and our result for the glass transition temperature T_g of polypropylene

Method	System	T_g [K]
Experimental	aPP	266 [61]
	iPP	272 [61]
		282.3 [65]
Molecular Dynamics Simulation	aPP192(1)	270* [66]
	PP100(1)**	248 [62]
	aPP90(8)	364 [64]
	iPP100(1)	282.1 [65]
This study	iPP240(4)	273.66 ± 4.21

*The value is not mentioned in the text of the reference. It is taken from Fig. 6 of [66]

**The tacticity is not specified in the text

Conclusions

We have studied the behaviour and interaction of different penetrants within polypropylene by means of molecular dynamics (MD) and Grand Canonical Monte Carlo (GCMC) simulations by considering isotactic polypropylene (iPP) and in one case atactic polypropylene (aPP) as well. For the polar penetrant water (H_2O) we find clusters forming and persisting over the whole simulation time length of 11 ns. This is consistent with previous results [19, 20]. Furthermore, for the first time we have also studied the diffusion of hydrogen peroxide (H_2O_2) in PP over a simulation time length of 22 ns which shows similar robust clustering as H_2O.

Diffusion coefficients for H_2O and oxygen (O_2) in iPP as well as for hydrogen (H_2) in iPP and aPP have been estimated by mean-square displacement (MSD) analysis of different time intervals up to 11 ns and for H_2O_2 in iPP for up to 22 ns. The MSD curves of polar penetrants are more volatile compared to the non-polar penetrants which imposes a larger uncertainty of the obtained results. For the case of oxygen, we first determined the glass transition temperature of iPP and further studied the influence of the glassy state and rubbery state of iPP on the diffusion coefficient as well. Our results are consistent with previously published experimental and computational data except for H_2 in polypropylene where our results are up to two orders of magnitude larger than other computational [14] and experimental results [57], respectively.

Sorption loading analysis on H_2O, O_2 and H_2 for iPP were performed and saturations were calculated. For H_2O our results are consistent with experimental results [59, 60]. However, due to different hindering effects like the polarity of H_2O, autoxidation for O_2 and the small size of H_2 molecules these systems are difficult to study experimentally which may explain the observed differences.

Declarations

Conflicts of interests The authors declare no conflict of interests.

References

1. GlobeNewswire (2019) Production volume of polypropylene resin worldwide in 2018 and 2026 (in million metric tons) [Graph]: In Statista. https://www.statista.com/statistics/1103529/global-polypropylene-production/. Accessed 16 May 2022

2. Shibryaeva L (2012) Thermal Oxidation of Polypropylene and Modified Polypropylene – Structure Effects // Modified Atmosphere Packaging for Perishable Plant Products. INTECH Open Access Publisher

3. Pielichowski K, Njuguna J (2005) Thermal degradation of polymeric materials. The Printing House, Crewe, UK

4. Trohalaki S, Rigby D, Kloczkowski A et al (1989) Estimation of diffusion coefficients for CO2 in polyethylene by molecular dynamics simulation. J Am Chem Soc Div Polym Chem 30:220–232

5. Takeuchi H, Okazaki K (1990) Molecular dynamics simulation of diffusion of simple gas molecules in a short chain polymer. J Chem Phys 92:5643–5652. https://doi.org/10.1063/1.458496

6. Takeuchi H (1990) A jump motion of small molecules in glassy polymers: A molecular dynamics simulation. J Chem Phys 93:2062–2067. https://doi.org/10.1063/1.459083

7. Takeuchi H (1990) Molecular dynamics simulations of diffusion of small molecules in polymers: Effect of chain length. J Chem Phys 93:4490–4491. https://doi.org/10.1063/1.458689

8. Madkour TM, Kloczkowski A, Mark JE et al (1992) Molecular dynamics investigations into the high permeability of siloxane polymers. Mater Res Soc Symp Proc 278:33–40

9. Boyd RH, Pant PVK (1991) Molecular packing and diffusion in polyisobutylene. Macromol 24:6325–6331. https://doi.org/10.1021/ma00023a040

10. Pant PVK, Boyd RH (1992) Simulation of diffusion of small-molecule penetrants in polymers. Macromol 25:494–495. https://doi.org/10.1021/ma00027a079

11. Pant PVK, Boyd RH (1993) Molecular-dynamics simulation of diffusion of small penetrants in polymers. Macromol 26:679–686. https://doi.org/10.1021/ma00056a019

12. Han J, Boyd RH (1994) Small-molecule penetrant diffusion in hydrocarbon polymers as studied by molecular dynamics simulation. Macromol 27:5365–5370. https://doi.org/10.1021/ma00097a016

13. Müller-Plathe F (1991) Diffusion of penetrants in amorphous polymehanrs: A molecular dynamics study. J Chem Phys 94:3192–3199. https://doi.org/10.1063/1.459788

14. Müller-Plathe F (1992) Molecular dynamics simulation of gas transport in amorphous polypropylene. J Chem Phys 96:3200–3205. https://doi.org/10.1063/1.461963

15. Müller-Plathe F, Rogers SC, van Gunsteren WF (1992) Diffusion coefficients of penetrant gases in polyisobutylene can be calculated correctly by molecular-dynamics simulations. Macromol. https://doi.org/10.1021/ma00050a054

16. Müller-Plathe F, Rogers SC, van Gunsteren WF (1993) Gas sorption and transport in polyisobutylene: Equilibrium and nonequilibrium molecular dynamics simulations. J Chem Phys 98:9895–9904. https://doi.org/10.1063/1.464369

17. Tamai Y, Tanaka H, Nakanishi K (1994) Molecular simulation of permeation of small penetrants through membranes. 1. Diffusion Coefficients Macromol 27:4498–4508. https://doi.org/10.1021/ma00094a011

18. Tamai Y, Tanaka H, Nakanishi K (1995) Molecular design of polymer membranes using molecular simulation technique. Fluid Phase Equilib 104:363–374. https://doi.org/10.1016/0378-3812(94)02661-J

19. Fukuda M, Kuwajima S (1997) Molecular-dynamics simulation of moisture diffusion in polyethylene beyond 10 ns duration. J Chem Phys 107:2149–2159. https://doi.org/10.1063/1.474564

20. Fukuda M, Kuwajima S (1998) Molecular dynamics simulation of water diffusion in atactic and amorphous isotactic polypropylene. J Chem Phys 108:3001–3009. https://doi.org/10.1063/1.475686

21. Chang-Gui T, Hai-Jun F, Jian Z, Ling-Hong L, Xiao-Hua L (2009) Molecular simulation of oxygen adsorption and diffusion in polypropylene. Acta Phys Chim Sin 25:1373–1378

22. Rong L, Zhang G, Yang S (2010) Molecular simulation of oxygen diffusion in polymers. Proceedings of the 17th IAPRI World Conference on Packaging

23. Börjesson A, Erdtman E, Ahlström P et al (2013) Molecular modelling of oxygen and water permeation in polyethylene. Polym 54:2988–2998. https://doi.org/10.1016/j.polymer.2013.03.065

24. Sun B, Lu L, Zhu Y (2019) Molecular dynamics simulation on the diffusion of flavor, O2 and H2O molecules in LDPE film. Materials 12:3515. https://doi.org/10.3390/ma12213515

25. Tjell AØ, Almdal K (2018) Diffusion rate of hydrogen peroxide through water-swelled polyurethane membranes. Sens Bio-Sens Res 21:35–39. https://doi.org/10.1016/j.sbsr.2018.10.001

26. Yabuta K, Futamura H, Kawasaki K et al (2020) Impact of H2O2 sorption by polymers on the duration of aeration in pharmaceutical decontamination. J Pharm Sci 109:2767–2773. https://doi.org/10.1016/j.xphs.2020.05.024

27. Grauschopf U, Thomas K, Luemkemann J et al (2018) Line sterilization considerations and VHP. In: Warne NW, Mahler H-C (eds) Challenges in Protein Product Development, vol 38. Springer International Publishing, Cham, pp 385–406

28. Dietrick HJ, Meeks WW (1959) Permeability of various polymers to 90% hydrogen peroxide. J Appl Polym Sci 2:231–235. https://doi.org/10.1002/app.1959.070020518

29. Radl S, Larisegger S, Suzzi D et al (2011) Quantifying Absorption Effects during Hydrogen Peroxide Decontamination. J Pharm Innov 6:202–216. https://doi.org/10.1007/s12247-011-9114-6

30. BIOVIA (2020) Dassault systèmes, materials studio 20.1. San Diego: Dassault Systèmes

31. Sun H (1998) COMPASS: an ab initio force-field optimized for condensed-phase applications-overview with details on alkene and benzene compounds. J Phys Chem B. https://doi.org/10.1021/jp980939v

32. Hill JR, Sauer J (1994) Molecular mechanics potential for silica and zeolite catalysts based on ab initio calculations. 1. Dense and microporous silica. J Phys Chem 98:1238–1244. https://doi.org/10.1021/j100055a032

33. Hill JR, Sauer J (1995) Molecular mechanics potential for silica and zeolite catalysts based on ab initio calculations. 2. Aluminosilicates. J Phys Chem 99:9536–9550. https://doi.org/10.1021/j100023a036

34. Maple JR, Dinur U, Hagler AT (1988) Derivation of force fields for molecular mechanics and dynamics from ab initio energy surfaces. Proc Natl Acad Sci USA 85:5350–5354. https://doi.org/10.1073/pnas.85.15.5350

35. Maple JR, Hwang MJ, Stockfisch TP (1994) Derivation of class II force fields. I. Methodology and quantum force field for the alkyl functional group and alkane molecules. J Comput Chem 15:162–182. https://doi.org/10.1002/jcc.540150207

36. Hwang MJ, Stockfisch TP, Hagler AT (1994) Derivation of class II force fields. 2. Derivation and characterization of a class II force field, CFF93, for the alkyl functional group and alkane molecules. J Am Chem Soc 116:2515–2525. https://doi.org/10.1021/ja00085a036

37. Asche TS, Behrens P, Schneider AM (2017) Validation of the COMPASS force field for complex inorganic–organic hybrid polymers. J Sol-Gel Sci Technol 81:195–204. https://doi.org/10.1007/s10971-016-4185-y

38. Savin AV, Mazo MA (2020) The COMPASS force field: Validation for carbon nanoribbons. Physica E: Low Dimens Syst Nanostruct 118:113937. https://doi.org/10.1016/j.physe.2019.113937

39. Ionescu TC, Qi F, McCabe C et al (2006) Evaluation of force fields for molecular simulation of polyhedral oligomeric silsesquioxanes. J Phys Chem B 110:2502–2510. https://doi.org/10.1021/jp052707j

40. Chen XP, Yuan CA, Wong CK et al (2011) Validation of force-fields in predicting the physical and thermophysical properties of emeraldine base polyaniline. Mol Simul 37:990–996. https://doi.org/10.1080/08927022.2011.562503

41. Wang Q, Tang C, Li X et al (2017) Comparison of COMPASS and PCFF in calculating mechanical behaviors of aramid fiber by means of molecular dynamics. Model Meas Control B 86:438–446. https://doi.org/10.18280/mmc_b.860209

42. Wang X, Tang C, Wang Q et al (2017) Selection of optimal polymerization degree and force field in the molecular dynamics simulation of insulating paper cellulose. Energies 10:1377. https://doi.org/10.3390/en10091377

43. Sun H, Jin Z, Yang C et al (2016) COMPASS II: extended coverage for polymer and drug-like molecule databases. J Mol Model 22:47. https://doi.org/10.1007/s00894-016-2909-0

44. Sun H, Ren P, Fried J (1998) The COMPASS force field: parametrization and validation for phosphazenes. Comput Theor Polym Sci 8:229–246. https://doi.org/10.1016/S1089-3156(98)00042-7

45. McQuaid MJ, Sun H, Rigby D (2004) Development and validation of COMPASS force field parameters for molecules with aliphatic azide chains. J Comput Chem 25:61–71. https://doi.org/10.1002/jcc.10316

46. Yang J, Ren Y, Tian A et al (2000) COMPASS force field for 14 inorganic molecules, He, Ne, Ar, Kr, Xe, H2, O2, N2, NO, CO, CO2, NO2, CS2, and SO2, in liquid phases. J Phys Chem B 104:4951–4957. https://doi.org/10.1021/jp992913p

47. Akkermans RLC, Spenley NA, Robertson SH (2020) COMPASS III: automated fitting workflows and extension to ionic liquids. Mol Simul 47:540–551. https://doi.org/10.1080/08927022.2020.1808215

48. Theodorou DN, Suter UW (1985) Shape of unperturbed linear polymers: Polypropylene. Macromol 18:1206–1214. https://doi.org/10.1021/ma00148a028

49. Einstein A (1908) Elementare theorie der brownschen bewegung. Z Elektrochem 14:235–239. https://doi.org/10.1002/bbpc.19080141703

50. Gusev AA, Müller-Plathe F, van Gunsteren WF et al (1994) Dynamics of small molecules in bulk polymers. In: Monnerie L, Suter UW (eds) Atomistic modeling of physical properties, pp 207–247. https://doi.org/10.1007/BFb0080200

51. Simperler A, Kornherr A, Chopra R et al (2006) Glass transition temperature of glucose, sucrose, and trehalose: an experimental and in silico study. J Phys Chem B 110:19678–19684. https://doi.org/10.1021/jp063134t

52. Yu C-Y, Yang Z-Z (2011) A systemic investigation of hydrogen peroxide clusters (H2O2)n (n = 1–6) and liquid-state hydrogen peroxide: based on atom-bond electronegativity equalization method fused into molecular mechanics and molecular dynamics. J Phys Chem A 115:2615–2626

53. Willow SY, Salim MA, Kim KS, Hirata S (2015) Ab initio molecular dynamics of liquid water using embedded-fragment second-order many-body perturbation theory towards its accurate property prediction. Sci Rep 5:14358

54. Kiryushkin SG, Gromov BA (1972) Measurement of the diffusion coefficient of oxygen in a polymeric substance. Polym Sci USSR A 14:1715–1717. https://doi.org/10.1016/0032-3950(72)90045-7

55. Eken M, Turhan Ş, Kaptan Y et al (1995) Diffusion of oxygen into irradiated polypropylene films. Radiat Phys Chem 46:809–812. https://doi.org/10.1016/0969-806X(95)00267-2

56. van Gunsteren WF, Berendsen HJC (1987) Groningen molecular simulation (GROMOS) library manual, The Netherlands

57. Jeschke D, Stuart HA (1961) Diffusion und Permation von Gasen in Hochpolymeren in Abhängigkeit vom Kristallisationsgrad und von der Temperatur. Z Naturforsch 16a:37–50. https://doi.org/10.1515/zna-1961-0109

58. Kahraman R, Abu-Sharkh B (2007) Moisture absorption behavior of palm/polypropylene composites in distilled water and sea water. Int J Polym Mater Polym Biomater 56:43–53. https://doi.org/10.1080/00914030600701926

59. Deng H, Reynolds CT, Cabrera NO et al (2010) The water absorption behaviour of all-polypropylene composites and its effect on mechanical properties. Compos B Eng 41:268–275. https://doi.org/10.1016/j.compositesb.2010.02.007

60. Mat-Shayuti MS, Abdullah MZ, Megat-Yusoff PSM (2013) Water absorption properties and morphology of polypropylene/ polycarbonate/polypropylene-graft-maleic anhydride blends. Asian J Sci Res 6:167–176. https://doi.org/10.3923/ajsr.2013.167.176

61. Cowie JMG (1973) Glass transition temperatures of stereoblock, isotactic and atactic polypropylenes of various chain lengths. Eur Polym J 9:1041–1049. https://doi.org/10.1016/0014-3057(73)90081-5

62. Yu K-Q, Li Z-S, Sun J (2001) Polymer structures and glass transition: a molecular dynamics simulation study. Macromol Theory Simul 10:624–633. https://doi.org/10.1002/1521-3919(20010701)10:6%3c624::AID-MATS624%3e3.0.CO;2-K

63. Origin (2021) Version 2021b. https://www.originlab.com/doc/Tutorials/Fitting-Piecewise-Linear. Accessed 16 May 2022

64. Yu X, Wu R, Yang X (2010) Molecular dynamics study on glass transitions in atactic-polypropylene bulk and freestanding thin films. J Phys Chem B 114:4955–4963. https://doi.org/10.1021/jp910245k

65. Pokharel P, Wei F, Shi J et al (2021) Thermomechanical properties of polypropylene and styrene-ethylene-butylene-styrene blends:

a molecular simulation and experimental study. Soft Condensed Matter. https://doi.org/10.48550/arXiv.2101.03426

66. Han J, Gee RH, Boyd RH (1994) Glass transition temperatures of polymers from molecular dynamics simulations. Macromol 27:7781–7784. https://doi.org/10.1021/ma00104a036